

Centrality dependence of low-momentum direct-photon production in Au+Au collisions at $\sqrt{s_{NN}} = 200$ GeV

- A. Adare,¹³ S. Afanasiev,³¹ C. Aidala,^{40, 44, 45} N.N. Ajitanand,⁶³ Y. Akiba,^{57, 58} R. Akimoto,¹² H. Al-Bataineh,⁵¹ H. Al-Ta'ani,⁵¹ J. Alexander,⁶³ A. Angerami,¹⁴ K. Aoki,^{36, 57} N. Apadula,⁶⁴ Y. Aramaki,^{12, 57} H. Asano,^{36, 57} E.C. Aschenauer,⁷ E.T. Atomssa,^{37, 64} R. Averbeck,⁶⁴ T.C. Awes,⁵³ B. Azmoun,⁷ V. Babintsev,²⁵ M. Bai,⁶ G. Baksay,²⁰ L. Baksay,²⁰ B. Bannier,⁶⁴ K.N. Barish,⁸ B. Bassalleck,⁵⁰ A.T. Basye,¹ S. Bathe,^{5, 8, 58} V. Baublis,⁵⁶ C. Baumann,⁴⁶ S. Baumgart,⁵⁷ A. Bazilevsky,⁷ S. Belikov,^{7, *} R. Belmont,⁶⁸ R. Bennett,⁶⁴ A. Berdnikov,⁶⁰ Y. Berdnikov,⁶⁰ A.A. Bickley,¹³ X. Bing,⁵² D.S. Blau,³⁵ J.S. Bok,⁷² K. Boyle,^{58, 64} M.L. Brooks,⁴⁰ H. Buesching,⁷ V. Bumazhnov,²⁵ G. Bunce,^{7, 58} S. Butsyk,^{40, 50} C.M. Camacho,⁴⁰ S. Campbell,⁶⁴ P. Castera,⁶⁴ C.-H. Chen,⁶⁴ C.Y. Chi,¹⁴ M. Chiu,⁷ I.J. Choi,^{26, 72} J.B. Choi,¹⁰ S. Choi,⁶² R.K. Choudhury,⁴ P. Christiansen,⁴² T. Chujo,⁶⁷ P. Chung,⁶³ O. Chvala,⁸ V. Cianciolo,⁵³ Z. Citron,⁶⁴ B.A. Cole,¹⁴ M. Connors,⁶⁴ P. Constantin,⁴⁰ M. Csanád,¹⁸ T. Csörgő,⁷¹ T. Dahms,⁶⁴ S. Dairaku,^{36, 57} I. Danchev,⁶⁸ K. Das,²¹ A. Datta,⁴⁴ M.S. Daugherty,¹ G. David,⁷ A. Denisov,²⁵ A. Deshpande,^{58, 64} E.J. Desmond,⁷ K.V. Dharmawardane,⁵¹ O. Dietzsch,⁶¹ L. Ding,²⁹ A. Dion,^{29, 64} M. Donadelli,⁶¹ O. Drapier,³⁷ A. Drees,⁶⁴ K.A. Drees,⁶ J.M. Durham,^{40, 64} A. Durum,²⁵ D. Dutta,⁴ L. D'Orazio,⁴³ S. Edwards,^{6, 21} Y.V. Efremenko,⁵³ F. Ellinghaus,¹³ T. Engelmöre,¹⁴ A. Enokizono,^{39, 53} H. En'yo,^{57, 58} S. Esumi,⁶⁷ K.O. Eyser,⁸ B. Fadem,⁴⁷ D.E. Fields,⁵⁰ M. Finger,⁹ M. Finger, Jr.,⁹ F. Fleuret,³⁷ S.L. Fokin,³⁵ Z. Fraenkel,^{70, *} J.E. Frantz,^{52, 64} A. Franz,⁷ A.D. Frawley,²¹ K. Fujiwara,⁵⁷ Y. Fukao,⁵⁷ T. Fusayasu,⁴⁹ K. Gaiety,¹ C. Gal,⁶⁴ A. Garishvili,⁶⁵ I. Garishvili,^{39, 65} A. Glenn,^{13, 39} H. Gong,⁶⁴ X. Gong,⁶³ M. Gonin,³⁷ Y. Goto,^{57, 58} R. Granier de Cassagnac,³⁷ N. Grau,^{2, 14} S.V. Greene,⁶⁸ M. Grosse Perdekamp,^{26, 58} T. Gunji,¹² L. Guo,⁴⁰ H.-Å. Gustafsson,^{42, *} T. Hachiya,⁵⁷ J.S. Haggerty,⁷ K.I. Hahn,¹⁹ H. Hamagaki,¹² J. Hamblen,⁶⁵ R. Han,⁵⁵ J. Hanks,¹⁴ E.P. Hartouni,³⁹ K. Hashimoto,^{57, 59} E. Haslum,⁴² R. Hayano,¹² X. He,²² M. Heffner,³⁹ T.K. Hemmick,⁶⁴ T. Hester,⁸ J.C. Hill,²⁹ M. Hohlmann,²⁰ R.S. Hollis,⁸ W. Holzmann,¹⁴ K. Homma,²⁴ B. Hong,³⁴ T. Horaguchi,^{24, 67} Y. Hori,¹² D. Hornback,⁶⁵ S. Huang,⁶⁸ T. Ichihara,^{57, 58} R. Ichimiya,⁵⁷ J. Ide,⁴⁷ H. Inuma,³³ Y. Ikeda,^{57, 67} K. Imai,^{30, 36, 57} J. Imrek,¹⁷ M. Inaba,⁶⁷ A. Iordanova,⁸ D. Isenhower,¹ M. Ishihara,⁵⁷ T. Isobe,^{12, 57} M. Issah,⁶⁸ A. Isupov,³¹ D. Ivanischev,⁵⁶ D. Ivanishchev,⁵⁶ B.V. Jacak,⁶⁴ M. Javani,²² J. Jia,^{7, 63} X. Jiang,⁴⁰ J. Jin,¹⁴ B.M. Johnson,⁷ K.S. Joo,⁴⁸ D. Jouan,⁵⁴ D.S. Jumper,^{1, 26} F. Kajihara,¹² S. Kametani,⁵⁷ N. Kamihara,⁵⁸ J. Kamin,⁶⁴ S. Kaneti,⁶⁴ B.H. Kang,²³ J.H. Kang,⁷² J.S. Kang,²³ J. Kapustinsky,⁴⁰ K. Karatsu,^{36, 57} M. Kasai,^{57, 59} D. Kawall,^{44, 58} M. Kawashima,^{57, 59} A.V. Kazantsev,³⁵ T. Kempel,²⁹ A. Khanzadeev,⁵⁶ K.M. Kijima,²⁴ B.I. Kim,³⁴ C. Kim,³⁴ D.H. Kim,⁴⁸ D.J. Kim,³² E. Kim,⁶² E.-J. Kim,¹⁰ H.J. Kim,⁷² K.-B. Kim,¹⁰ S.H. Kim,⁷² Y.-J. Kim,²⁶ Y.K. Kim,²³ E. Kinney,¹³ K. Kiriluk,¹³ Á. Kiss,¹⁸ E. Kistenev,⁷ J. Klatsky,²¹ D. Kleinjan,⁸ P. Kline,⁶⁴ L. Kochenda,⁵⁶ Y. Komatsu,¹² B. Komkov,⁵⁶ M. Konno,⁶⁷ J. Koster,²⁶ D. Kotchetkov,^{50, 52} D. Kotov,^{56, 60} A. Kozlov,⁷⁰ A. Král,¹⁵ A. Kravitz,¹⁴ F. Krizek,³² G.J. Kunde,⁴⁰ K. Kurita,^{57, 59} M. Kurosawa,⁵⁷ Y. Kwon,⁷² G.S. Kyle,⁵¹ R. Lacey,⁶³ Y.S. Lai,¹⁴ J.G. Lajoie,²⁹ A. Lebedev,²⁹ B. Lee,²³ D.M. Lee,⁴⁰ J. Lee,¹⁹ K. Lee,⁶² K.B. Lee,³⁴ K.S. Lee,³⁴ S.H. Lee,⁶⁴ S.R. Lee,¹⁰ M.J. Leitch,⁴⁰ M.A.L. Leite,⁶¹ M. Leitgab,²⁶ E. Leitner,⁶⁸ B. Lenzi,⁶¹ B. Lewis,⁶⁴ X. Li,¹¹ P. Liebing,⁵⁸ S.H. Lim,⁷² L.A. Linden Levy,¹³ T. Liška,¹⁵ A. Litvinenko,³¹ H. Liu,^{40, 51} M.X. Liu,⁴⁰ B. Love,⁶⁸ R. Luechtenborg,⁴⁶ D. Lynch,⁷ C.F. Maguire,⁶⁸ Y.I. Makdisi,⁶ M. Makey,^{70, 73} A. Malakhov,³¹ M.D. Malik,⁵⁰ A. Manion,⁶⁴ V.I. Manko,³⁵ E. Mannel,¹⁴ Y. Mao,^{55, 57} H. Masui,⁶⁷ S. Masumoto,¹² F. Matathias,¹⁴ M. McCumber,^{13, 64} P.L. McGaughey,⁴⁰ D. McGlinchey,^{13, 21} C. McKinney,²⁶ N. Means,⁶⁴ M. Mendoza,⁸ B. Meredith,²⁶ Y. Miake,⁶⁷ T. Mibe,³³ A.C. Mignerey,⁴³ P. Mikeš,^{9, 28} K. Miki,^{57, 67} A. Milov,^{7, 70} D.K. Mishra,⁴ M. Mishra,³ J.T. Mitchell,⁷ Y. Miyachi,^{57, 66} S. Miyasaka,^{57, 66} A.K. Mohanty,⁴ H.J. Moon,⁴⁸ Y. Morino,¹² A. Morreale,⁸ D.P. Morrison,^{7, †} S. Motschwiller,⁴⁷ T.V. Moukhanova,³⁵ T. Murakami,^{36, 57} J. Murata,^{57, 59} T. Nagae,³⁶ S. Nagamiya,^{33, 57} J.L. Nagle,^{13, ‡} M. Naglis,⁷⁰ M.I. Nagy,^{18, 71} I. Nakagawa,^{57, 58} Y. Nakamiya,²⁴ K.R. Nakamura,^{36, 57} T. Nakamura,^{33, 57} K. Nakano,^{57, 66} C. Nattrass,⁶⁵ A. Nederlof,⁴⁷ J. Newby,³⁹ M. Nguyen,⁶⁴ M. Nihashi,^{24, 57} R. Nouicer,^{7, 58} N. Novitzky,³² A.S. Nyanin,³⁵ E. O'Brien,⁷ S.X. Oda,¹² C.A. Ogilvie,²⁹ M. Oka,⁶⁷ K. Okada,⁵⁸ Y. Onuki,⁵⁷ A. Oskarsson,⁴² M. Ouchida,^{24, 57} K. Ozawa,¹² R. Pak,⁷ V. Pantuev,^{27, 64} V. Papavassiliou,⁵¹ B.H. Park,²³ I.H. Park,¹⁹ J. Park,⁶² S.K. Park,³⁴ W.J. Park,³⁴ S.F. Pate,⁵¹ L. Patel,²² H. Pei,²⁹ J.-C. Peng,²⁶ H. Pereira,¹⁶ V. Peresedov,³¹ D.Yu. Peressounko,³⁵ R. Petti,⁶⁴ C. Pinkenburg,⁷ R.P. Pisani,⁷ M. Proissl,⁶⁴ M.L. Purschke,⁷ A.K. Purwar,⁴⁰ H. Qu,^{1, 22} J. Rak,³² A. Rakotozafindrabe,³⁷ I. Ravinovich,⁷⁰ K.F. Read,^{53, 65} K. Reygers,⁴⁶ D. Reynolds,⁶³ V. Riabov,⁵⁶ Y. Riabov,^{56, 60} E. Richardson,⁴³ N. Riveli,⁵² D. Roach,⁶⁸ G. Roche,⁴¹ S.D. Rolnick,⁸ M. Rosati,²⁹ C.A. Rosen,¹³ S.S.E. Rosendahl,⁴² P. Rosnet,⁴¹ P. Rukoyatkin,³¹ P. Ružička,²⁸ B. Sahlmueller,^{46, 64} N. Saito,³³ T. Sakaguchi,⁷ K. Sakashita,^{57, 66} V. Samsonov,⁵⁶ M. Sano,⁶⁷ S. Sano,^{12, 69} M. Sarsour,²² T. Sato,⁶⁷ S. Sawada,³³ K. Sedgwick,⁸ J. Seele,¹³

R. Seidl,^{26, 57, 58} A.Yu. Semenov,²⁹ A. Sen,²² R. Seto,⁸ D. Sharma,⁷⁰ I. Shein,²⁵ T.-A. Shibata,^{57, 66} K. Shigaki,²⁴ M. Shimomura,⁶⁷ K. Shoji,^{36, 57} P. Shukla,⁴ A. Sickles,⁷ C.L. Silva,^{29, 61} D. Silvermyr,⁵³ C. Silvestre,¹⁶ K.S. Sim,³⁴ B.K. Singh,³ C.P. Singh,³ V. Singh,³ M. Slunečka,⁹ R.A. Soltz,³⁹ W.E. Sondheim,⁴⁰ S.P. Sorensen,⁶⁵ M. Soumya,⁶³ I.V. Sourikova,⁷ N.A. Sparks,¹ P.W. Stankus,⁵³ E. Stenlund,⁴² M. Stepanov,⁴⁴ A. Ster,⁷¹ S.P. Stoll,⁷ T. Sugitate,²⁴ A. Sukhanov,⁷ J. Sun,⁶⁴ J. Sziklai,⁷¹ E.M. Takagui,⁶¹ A. Takahara,¹² A. Taketani,^{57, 58} R. Tanabe,⁶⁷ Y. Tanaka,⁴⁹ S. Taneja,⁶⁴ K. Tanida,^{36, 57, 58, 62} M.J. Tannenbaum,⁷ S. Tarafdar,³ A. Taranenko,⁶³ P. Tarján,¹⁷ E. Tennant,⁵¹ H. Themann,⁶⁴ T.L. Thomas,⁵⁰ T. Todoroki,^{57, 67} M. Togawa,^{36, 57} A. Toia,⁶⁴ L. Tomášek,²⁸ M. Tomášek,^{15, 28} H. Torii,²⁴ R.S. Towell,¹ I. Tserruya,⁷⁰ Y. Tsuchimoto,^{12, 24} T. Tsuji,¹² C. Vale,^{7, 29} H. Valle,⁶⁸ H.W. van Hecke,⁴⁰ M. Vargyas,¹⁸ E. Vazquez-Zambrano,¹⁴ A. Veicht,^{14, 26} J. Velkovska,⁶⁸ R. Vértesi,^{17, 71} A.A. Vinogradov,³⁵ M. Virius,¹⁵ A. Vossen,²⁶ V. Vrba,^{15, 28} E. Vznuzdaev,⁵⁶ X.R. Wang,⁵¹ D. Watanabe,²⁴ K. Watanabe,⁶⁷ Y. Watanabe,^{57, 58} Y.S. Watanabe,¹² F. Wei,²⁹ R. Wei,⁶³ J. Wessels,⁴⁶ S. Whitaker,²⁹ S.N. White,⁷ D. Winter,¹⁴ S. Wolin,²⁶ J.P. Wood,¹ C.L. Woody,⁷ R.M. Wright,¹ M. Wysocki,¹³ W. Xie,⁵⁸ Y.L. Yamaguchi,^{12, 57} K. Yamaura,²⁴ R. Yang,²⁶ A. Yanovich,²⁵ J. Ying,²² S. Yokkaichi,^{57, 58} Z. You,^{40, 55} G.R. Young,⁵³ I. Younus,^{38, 50} I.E. Yushmanov,³⁵ W.A. Zajc,¹⁴ A. Zelenski,⁶ C. Zhang,⁵³ S. Zhou,¹¹ and L. Zolin³¹

(PHENIX Collaboration)

¹Abilene Christian University, Abilene, Texas 79699, USA

²Department of Physics, Augustana College, Sioux Falls, South Dakota 57197, USA

³Department of Physics, Banaras Hindu University, Varanasi 221005, India

⁴Bhabha Atomic Research Centre, Bombay 400 085, India

⁵Baruch College, City University of New York, New York, New York, 10010 USA

⁶Collider-Accelerator Department, Brookhaven National Laboratory, Upton, New York 11973-5000, USA

⁷Physics Department, Brookhaven National Laboratory, Upton, New York 11973-5000, USA

⁸University of California - Riverside, Riverside, California 92521, USA

⁹Charles University, Ovocný trh 5, Praha 1, 116 36, Prague, Czech Republic

¹⁰Chonbuk National University, Jeonju, 561-756, Korea

¹¹Science and Technology on Nuclear Data Laboratory, China Institute of Atomic Energy, Beijing 102413, P. R. China

¹²Center for Nuclear Study, Graduate School of Science, University of Tokyo, 7-3-1 Hongo, Bunkyo, Tokyo 113-0033, Japan

¹³University of Colorado, Boulder, Colorado 80309, USA

¹⁴Columbia University, New York, New York 10027 and Nevis Laboratories, Irvington, New York 10533, USA

¹⁵Czech Technical University, Zikova 4, 166 36 Prague 6, Czech Republic

¹⁶Dapnia, CEA Saclay, F-91191, Gif-sur-Yvette, France

¹⁷Debrecen University, H-4010 Debrecen, Egyetem tér 1, Hungary

¹⁸ELTE, Eötvös Loránd University, H - 1117 Budapest, Pázmány P. s. 1/A, Hungary

¹⁹Ewha Womans University, Seoul 120-750, Korea

²⁰Florida Institute of Technology, Melbourne, Florida 32901, USA

²¹Florida State University, Tallahassee, Florida 32306, USA

²²Georgia State University, Atlanta, Georgia 30303, USA

²³Hanyang University, Seoul 133-792, Korea

²⁴Hiroshima University, Kagamiyama, Higashi-Hiroshima 739-8526, Japan

²⁵IHEP Protvino, State Research Center of Russian Federation, Institute for High Energy Physics, Protvino, 142281, Russia

²⁶University of Illinois at Urbana-Champaign, Urbana, Illinois 61801, USA

²⁷Institute for Nuclear Research of the Russian Academy of Sciences, prospekt 60-letiya Oktyabrya 7a, Moscow 117312, Russia

²⁸Institute of Physics, Academy of Sciences of the Czech Republic, Na Slovance 2, 182 21 Prague 8, Czech Republic

²⁹Iowa State University, Ames, Iowa 50011, USA

³⁰Advanced Science Research Center, Japan Atomic Energy Agency, 2-4

Shirakata Shirane, Tokai-mura, Naka-gun, Ibaraki-ken 319-1195, Japan

³¹Joint Institute for Nuclear Research, 141980 Dubna, Moscow Region, Russia

³²Helsinki Institute of Physics and University of Jyväskylä, P.O.Box 35, FI-40014 Jyväskylä, Finland

³³KEK, High Energy Accelerator Research Organization, Tsukuba, Ibaraki 305-0801, Japan

³⁴Korea University, Seoul, 136-701, Korea

³⁵Russian Research Center "Kurchatov Institute", Moscow, 123098 Russia

³⁶Kyoto University, Kyoto 606-8502, Japan

³⁷Laboratoire Leprince-Ringuet, Ecole Polytechnique, CNRS-IN2P3, Route de Saclay, F-91128, Palaiseau, France

³⁸Physics Department, Lahore University of Management Sciences, Lahore 54792, Pakistan

³⁹Lawrence Livermore National Laboratory, Livermore, California 94550, USA

⁴⁰Los Alamos National Laboratory, Los Alamos, New Mexico 87545, USA

⁴¹LPC, Université Blaise Pascal, CNRS-IN2P3, Clermont-Fd, 63177 Aubiere Cedex, France

⁴²Department of Physics, Lund University, Box 118, SE-221 00 Lund, Sweden

⁴³University of Maryland, College Park, Maryland 20742, USA

⁴⁴Department of Physics, University of Massachusetts, Amherst, Massachusetts 01003-9337, USA

- ⁴⁵Department of Physics, University of Michigan, Ann Arbor, Michigan 48109-1040, USA
⁴⁶Institut für Kernphysik, University of Muenster, D-48149 Muenster, Germany
⁴⁷Muhlenberg College, Allentown, Pennsylvania 18104-5586, USA
⁴⁸Myongji University, Yongin, Kyonggido 449-728, Korea
⁴⁹Nagasaki Institute of Applied Science, Nagasaki-shi, Nagasaki 851-0193, Japan
⁵⁰University of New Mexico, Albuquerque, New Mexico 87131, USA
⁵¹New Mexico State University, Las Cruces, New Mexico 88003, USA
⁵²Department of Physics and Astronomy, Ohio University, Athens, Ohio 45701, USA
⁵³Oak Ridge National Laboratory, Oak Ridge, Tennessee 37831, USA
⁵⁴IPN-Orsay, Universite Paris Sud, CNRS-IN2P3, BP1, F-91406, Orsay, France
⁵⁵Peking University, Beijing 100871, P. R. China
⁵⁶PNPI, Petersburg Nuclear Physics Institute, Gatchina, Leningrad region, 188300, Russia
⁵⁷RIKEN Nishina Center for Accelerator-Based Science, Wako, Saitama 351-0198, Japan
⁵⁸RIKEN BNL Research Center, Brookhaven National Laboratory, Upton, New York 11973-5000, USA
⁵⁹Physics Department, Rikkyo University, 3-34-1 Nishi-Ikebukuro, Toshima, Tokyo 171-8501, Japan
⁶⁰Saint Petersburg State Polytechnic University, St. Petersburg, 195251 Russia
⁶¹Universidade de São Paulo, Instituto de Física, Caixa Postal 66318, São Paulo CEP05315-970, Brazil
⁶²Department of Physics and Astronomy, Seoul National University, Seoul 151-742, Korea
⁶³Chemistry Department, Stony Brook University, SUNY, Stony Brook, New York 11794-3400, USA
⁶⁴Department of Physics and Astronomy, Stony Brook University, SUNY, Stony Brook, New York 11794-3800, USA
⁶⁵University of Tennessee, Knoxville, Tennessee 37996, USA
⁶⁶Department of Physics, Tokyo Institute of Technology, Oh-okayama, Meguro, Tokyo 152-8551, Japan
⁶⁷Institute of Physics, University of Tsukuba, Tsukuba, Ibaraki 305, Japan
⁶⁸Vanderbilt University, Nashville, Tennessee 37235, USA
⁶⁹Waseda University, Advanced Research Institute for Science and Engineering, 17 Kikui-cho, Shinjuku-ku, Tokyo 162-0044, Japan
⁷⁰Weizmann Institute, Rehovot 76100, Israel
⁷¹Institute for Particle and Nuclear Physics, Wigner Research Centre for Physics, Hungarian Academy of Sciences (Wigner RCP, RMKI) H-1525 Budapest 114, POBox 49, Budapest, Hungary
⁷²Yonsei University, IPAP, Seoul 120-749, Korea
⁷³University of Zagreb, Faculty of Science, Department of Physics, Bijenička 32, HR-10002 Zagreb, Croatia

(Dated: May 16, 2014)

The PHENIX experiment at RHIC has measured the centrality dependence of the direct photon yield from Au+Au collisions at $\sqrt{s_{NN}} = 200$ GeV down to $p_T = 0.4$ GeV/c. Photons are detected via photon conversions to e^+e^- pairs and an improved technique is applied that minimizes the systematic uncertainties that usually limit direct photon measurements, in particular at low p_T . We find an excess of direct photons above the N_{coll} -scaled yield measured in $p+p$ collisions. This excess yield is well described by an exponential distribution with an inverse slope of about 240 MeV/c in the p_T range from 0.6–2.0 GeV/c. While the shape of the p_T distribution is independent of centrality within the experimental uncertainties, the yield increases rapidly with increasing centrality, scaling approximately with N_{part}^α , where $\alpha = 1.48 \pm 0.08(\text{stat}) \pm 0.04(\text{syst})$.

PACS numbers: 25.75.Dw

I. INTRODUCTION

Photons are an excellent probe of the hot and dense, strongly interacting matter produced in heavy ion collisions [1]. They do not participate in the strong interaction and thus exit the system carrying information from the time of their emission, allowing a glimpse at the time-evolution of the matter. Experimentally we measure a time-integrated history of the emission. Photons from hadron decays need to be removed to reveal the so-called direct contribution, i.e. photons that are produced before

the formation of the matter as well as from the matter itself. Further removal of the early component, usually considered prompt production from $2 \rightarrow 2$ scattering of the partons from the incoming nuclei, gives access to the radiation emitted from the matter. If the matter is in local equilibrium the photon spectrum is a time-integrated image of the evolution of the temperature and collective motion of the matter as it expands and cools.

PHENIX discovered evidence of thermal photons from Au+Au collisions [2] at RHIC energies; similar findings have recently been reported by ALICE from Pb+Pb collisions at the Large Hadron Collider [3]. These photons exhibit a large yield and an azimuthal anisotropy [4, 5] with respect to the reaction plane, often referred to as elliptic flow and quantified as v_2 . Comparing the measured p_T spectra to model calculations of thermal photons based on a hydrodynamic evolution of the sys-

* Deceased

† PHENIX Co-Spokesperson: morrison@bnl.gov

‡ PHENIX Co-Spokesperson: jamie.nagle@colorado.edu

tem, microscopic transport models, or a more schematic time evolution gives reasonable agreement when assuming an initial temperature of 300 MeV or above [6–13] for $\sqrt{s_{NN}} = 200$ GeV Au+Au collisions at RHIC. However, it is a challenge for these types of models to simultaneously explain the large observed azimuthal anisotropy of the radiation and the large yield [13–17].

The challenge for these model calculations results from the interplay between the time evolution of the collective motion and the cooling of the matter that emits photons. In the model calculations the collective motion builds up over time. The flow velocity is initially small and increases throughout the collision as the matter continues to expand. The yield of thermal photons is expected to be largest early in the collision when the matter is the hottest. Theoretical models that create large v_2 typically underestimate the direct photon yield. Attempts to improve hydrodynamic models by implementing next-to-leading-order thermal rates [18], initial state fluctuations [13], formation time effects [17], increased radial flow and enhanced coupling at T_C [16], fail to reconcile yield and anisotropy.

To resolve this puzzle new production mechanisms have been proposed. Some enhance the thermal yield in the presence of the strong magnetic field perpendicular to the reaction plane, which creates a large anisotropy [19, 20]. Other new mechanisms, such as synchrotron radiation [21] at the plasma boundary or photon production in a glasma phase [22], create an anisotropy due to the initial geometry of the overlap region.

II. EXPERIMENT

In this paper we provide new information on the centrality dependence of the direct photon yield that will help to distinguish between different production mechanisms [23]. To measure the centrality dependence of the photon radiation, we analyzed large data samples of 1.4×10^9 and 2.6×10^9 minimum bias Au+Au collisions recorded with the PHENIX central arm spectrometers during the 2007 and 2010 runs, respectively. The main PHENIX detector is described in detail elsewhere [24]. In addition, a Hadron Blind Detector (HBD) [25] was installed, except for part of the 2007 RHIC run when only one half of the HBD was installed. The data were taken with a special field configuration which essentially cancels the magnetic field around the beam axis out to about 50 cm.

Minimum bias events were triggered using the beam-beam counters (BBC) that cover the rapidity region $3.1 < |\eta| < 3.9$ and 2π in azimuth in both beam directions. The BBC information is used to limit the vertex in beam direction to ± 10 cm around the nominal position. The charge measured in the BBC is used to categorize the event centrality. The sample is divided into four centrality classes, 0%–20% for the most central selection, 20%–40%, 40%–60% and 60%–92% for the most periph-

eral sample.

The raw inclusive photon yield N_γ^{incl} is measured through photon conversions to e^+e^- pairs in the detector material, which allows us to avoid hadron contamination and measure photons down to $p_T^{ee} = 0.4$ GeV/c. Trajectories and momenta of e^+ and e^- are determined using the drift chambers and the pad chambers that measure the deflection in the axial magnetic field. We require a minimum p_T of 200 GeV/c. The energy is determined with the electromagnetic calorimeter (EMCal). The e^+ and e^- are identified utilizing the ring-imaging Čerenkov detector by requiring a minimum of three phototubes associated with both charged tracks at the expected ring radius as well as requiring the respective energy/momentum ratios to be greater than 0.6, with the energy measured in the EMCal.

III. DATA ANALYSIS

For this analysis we select photons that converted at a well-defined location, namely in the readout plane of the HBD that is located at a radius of 60 cm and has a radiation length $X/X_0 \approx 2.5\%$. Because the standard PHENIX momentum reconstruction algorithm assumes that the e^+ and e^- tracks originate from the event vertex, the momenta of these conversion electrons are initially mismeasured; as a result the e^+e^- pair is reconstructed with an average mass of about $M_{\text{vtx}} \approx 12$ MeV/ c^2 , as is shown in the invariant pair mass distribution on panel (a) of Figure 1. The first peak in the mass plot at a few MeV/ c^2 is from π^0 Dalitz decays, along with a small number of pairs from photon conversions before the HBD readout plane.

The momenta of the conversion candidates are then recalculated assuming that the conversion occurred at the HBD readout plane. If the conversion indeed happened in the readout plane, the relative momentum resolution of the pair is approximately $\sigma_{p_T}^{ee}/p_T^{ee} = 0.9\% \oplus 0.5\% p_T^{ee}$. The e^+e^- pair mass M_{HBD} is a few MeV/ c^2 , consistent with the experimental resolution. For all other e^+e^- pairs from conversions happening elsewhere, and from Dalitz decays or other e^+e^- sources the mass is shifted upward. The recalculated mass spectrum is shown in panel (b) of Figure 1. Plotting the yield as function of mass recalculated with the HBD back plane as origin (M_{HBD}) versus the mass calculated with the vertex as origin (M_{vtx}), as shown in Figure 2, allows one to clearly isolate the conversions in the HBD readout plane. We select photon conversions by a two dimensional cut $10 < M_{\text{vtx}} < 15$ MeV/ c^2 and $M_{\text{HBD}} < 4.5$ MeV/ c^2 , illustrated by the red dashed box in the figure. Note that the large distance from the true event vertex and the relatively thick HBD readout plane (in terms of radiation length X_0) with no comparable radiating material nearby makes identification of the converted photons very accurate: a full GEANT Monte Carlo simulation shows that the purity of this sample is 99%, with most of the re-

maining 1% being photon conversions at other radii.

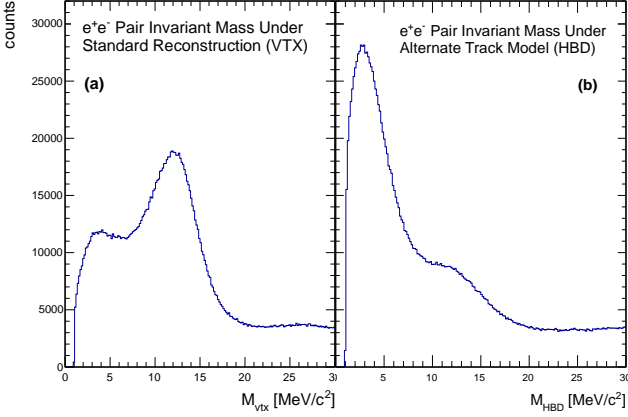


FIG. 1. Histograms of the e^+e^- pair invariant mass distribution from data. Panel (a) shows the distribution of masses calculated with the normal reconstruction algorithm (vtx). Panel (b) shows the distribution of masses calculated with the alternate track model assumption (HBD).

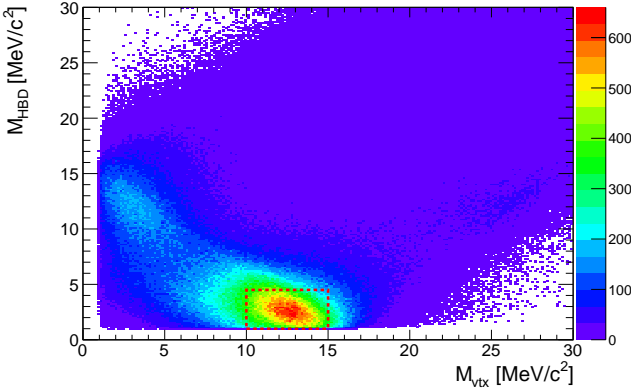


FIG. 2. A view of the cut space used for the conversion photon identification. The mass as calculated under the standard reconstruction algorithm (vtx) is plotted on the horizontal axis, while the mass as calculated under the alternate track model (HBD) is plotted on the vertical axis. The red dotted box indicates the region used to identify photon conversions.

A subset of this inclusive conversion photon sample N_{γ}^{incl} is tagged statistically as photons from π^0 decays if they reconstruct the π^0 mass with a second, photon-like shower taken from the EMCal. Note that this is done in bins of p_T^{ee} , the transverse momentum of the converted photons, not in bins of $\pi^0 p_T$. A cut on the shower shape of this second, EMCal shower is used to remove most hadrons. False tagging from hadron showers in the EMCal is further reduced by applying a lower threshold on the cluster energy. For the 2010 data we applied an $E_{\text{clus}} > 0.4$ GeV cut, which is just above the EMCal re-

sponse for minimum ionizing particles. For the 2007 data a higher threshold of 0.6 GeV was necessary due to a cut on the shower energy that was introduced during data production.

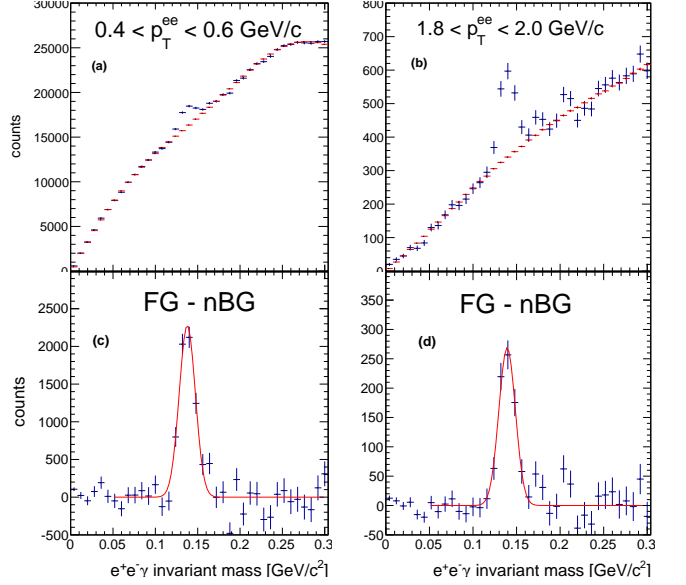


FIG. 3. Histograms of the $e^+e^-\gamma$ invariant mass distributions for two different p_T^{ee} bins. The left column (a),(c) displays the mass for $0.4 < p_T^{ee} < 0.6$ GeV/c, the right column (b),(d) displays the mass for $1.8 < p_T^{ee} < 2.0$ GeV/c. The top row (a),(b) shows the diphoton foreground distribution in blue, with the normalized background distribution from the mixed events in red. The bottom row (c),(d) shows the isolated pion peak after subtraction of the normalized background. The masses are calculated from the HBD readout plane origin assumption on the electron tracks. The centrality bin is 0%–20%.

A. Relative Photon Yield

In each p_T^{ee} bin the number of π^0 tagged photons ($N_{\gamma}^{\pi^0, \text{tag}}$) are determined by integrating the $e^+e^-\gamma$ mass distribution around the π^0 mass after subtraction of the mixed-event combinatorial background. Figure 3 shows the mass distributions before and after subtracting the mixed-event background for two example p_T^{ee} bins (0.4–0.6 GeV/c and 1.8–2.0 GeV/c) for central collisions (0%–20%), which have the smallest signal-to-background ratio. The π^0 peak extraction method has less than 4% systematic uncertainty on the π^0 tagged photon yield, which is assumed to be independent between neighboring p_T^{ee} bins and thus folded into the statistical uncertainties.

In a given p_T^{ee} bin the true number of inclusive photons γ^{incl} and photons from π^0 decays γ^{π^0} are related to the

measured quantities N_γ^{incl} and $N_\gamma^{\pi^0, \text{tag}}$ as follows:

$$N_\gamma^{\text{incl}} = \varepsilon_{ee} a_{ee} c \gamma^{\text{incl}}, \quad (1)$$

$$N_\gamma^{\pi^0, \text{tag}} = \varepsilon_{ee} a_{ee} c \langle \varepsilon_\gamma f \rangle \gamma^{\pi^0}, \quad (2)$$

where c is the probability that the photon converts in the HBD readout plane, ε_{ee} is the reconstruction efficiency of the e^+e^- pair and a_{ee} is the factor describing that both e^+ and e^- are in the detector acceptance. The factor f is the conditional acceptance that after one photon from a π^0 decay was reconstructed as e^+e^- conversion pair, the partner photon falls into the acceptance of the EMCal. The probability that the partner photon is reconstructed is given as ε_γ . The product $\varepsilon_\gamma f$ is averaged over all possible p_T of the partner photon, indicated by $\langle \varepsilon_\gamma f \rangle$.

Because N_γ^{incl} and $N_\gamma^{\pi^0, \text{tag}}$ are both measured in terms of the p_T^e of the converted photon, the efficiency and acceptance factors for the e^+e^- pair as well as the conversion probability explicitly cancel in the ratio $N_\gamma^{\text{incl}}/N_\gamma^{\pi^0, \text{tag}}$. This ratio can be converted into R_γ , the ratio of the yield of true inclusive photons γ^{incl} to the yield of true photons from hadron decays γ^{hadron} :

$$R_\gamma = \frac{\gamma^{\text{incl}}}{\gamma^{\text{hadron}}} = \frac{\langle \varepsilon_\gamma f \rangle \left(\frac{N_\gamma^{\text{incl}}}{N_\gamma^{\pi^0, \text{tag}}} \right)_{\text{Data}}}{\left(\frac{\gamma^{\text{hadron}}}{\gamma^{\pi^0}} \right)_{\text{Sim}}} \quad (3)$$

All terms in Eq. 3 are a function of converted photon p_T^e . R_γ will be unity for a given p_T^e bin if all photons result from hadron decays, or larger than unity if direct photons are present in the sample. The excess above unity is a measure of the direct photon content in the bin. In the following we discuss all terms in detail.

The numerator of Eq. 3 includes the measured ratio $N_\gamma^{\text{incl}}/N_\gamma^{\pi^0, \text{tag}}$, and the efficiency and acceptance correction for pion tagging, $\langle \varepsilon_\gamma f \rangle$. Two different methods are used to calculate $\langle \varepsilon_\gamma f \rangle$. For the 2007 data a GEANT Monte Carlo simulation of the detector response to π^0 decays is performed. In the simulation one photon is forced to convert in the HBD readout plane. The simulated π^0 decays are then embedded into real data to account for occupancy effects in the EMCal. The events are analyzed through the full reconstruction chain to extract $\langle \varepsilon_\gamma f \rangle$. This method is computationally very intensive and thus limited by statistical uncertainties. To overcome these we developed a fast simulation. It accounts for the detector acceptance and variations of the active detector areas with time. The single photon response is parameterized based on a GEANT Monte Carlo simulation of single photons. To test the fast simulation we compared its result for $\langle \varepsilon_\gamma f \rangle$ for the 2007 data to the one determined with the full GEANT simulation; the two methods agree within statistical uncertainties. For the 2010 data we used the fast simulation.

B. Systematic Uncertainties

Several sources contribute to systematic uncertainties on $\langle \varepsilon_\gamma f \rangle$. The largest one is 4% and accounts for the uncertainties of the energy scale and the energy resolution. These translate directly into an uncertainty in the number of photons that pass the lower EMCal threshold and thus become candidates for π^0 tagging. The second largest uncertainty (2%) is on the number of photons that are lost because they convert to e^+e^- pairs in the detector material in front of the EMCal and are not reconstructed as single showers. The active area of the detectors was studied as a function of time, and the resulting systematic uncertainty on $\langle \varepsilon_\gamma f \rangle$ is smaller than 1%. Varying the π^0 input distribution with the uncertainties on the data results in a 1% uncertainty on $\langle \varepsilon_\gamma f \rangle$. Lastly, the uncertainty on the photon reconstruction efficiency is also small (1%), estimated by varying the shower shape cuts, redoing the analysis and recalculating the correction, and comparing the results. All other systematic effects were found to be negligible.

The denominator of Eq. 3 is the ratio of photons from all hadron decays to those from π^0 decays. We evaluate the decay photon contributions from π^0 , η , ω , and η' mesons using a hadron decay generator that is based on experimental data for the parent hadrons measured in the same experiment for all hadrons listed except η' . Details are discussed in Ref. [26].

The branching ratios and decay kinematics are based on Ref. [27]. The shape of the spectra for η , ω , and η' are derived from the π^0 spectrum, where we assume m_T scaling by replacing p_T with $m_T = \sqrt{m_{\text{hadron}}^2 - m_{\pi^0}^2 + p_T^2}$. Because the π^0 contribution is 80% of γ^{hadron} (Eq. 3) the uncertainty on the π^0 spectra largely cancels, leaving the η/π^0 ratio as the dominant source of systematic uncertainties. We use a value of $\eta/\pi^0 = 0.46 \pm 0.06$ [28, 29] at $p_T = 5$ GeV/c to appropriately scale the η yield to that of pions. The uncertainty on R_γ also includes possible deviations from scaling with m_T and uncertainties on the other meson yields. The total uncertainty is less than 2.5%. All systematic uncertainties on R_γ are summarized in Table I.

IV. RESULTS AND DISCUSSION

Figure 4 compares our results for R_γ in minimum bias collisions from the 2007 and 2010 data sets separately, while Fig. 5 shows the same quantity for the four centrality selections. Here we used the full GEANT simulation for the 2007 data, and the fast Monte Carlo simulation for the 2010 data. R_γ from the two data sets agree well within statistical errors. In Fig. 5 we also included data from an earlier publication [2], in which R_γ was obtained by extrapolating virtual photons to $m = 0$ for the two central bins and $p_T > 1.0$ GeV/c. It was used to calculate the direct photon p_T spectra shown in [2]; here we

TABLE I. Summary of systematic uncertainties on R_γ . The π^0 reconstruction uncertainty is uncorrelated between data points (type A); type B uncertainties are p_T -correlated, type C uncertainties are an overall scale factor R_γ .

Source	$\sigma_{\text{syst}}/R_\gamma$	Type
π^0 reconstruction		
(tagged photon yield)	4%	A
γ purity	1%	C
conditional acceptance $\langle \varepsilon f \rangle$		
energy scale	4%	B
conversion loss	2%	C
γ efficiency	1%	B
active area	1%	C
input p_T spectra	1%	B
$\gamma^{\text{hadron}}/\gamma^{\pi^0}$		
η/π^0 ratio	2.2%	C
other mesons	<1%	C

show the corresponding R_γ data points. We observe no statistically significant difference between R_γ measured from real and virtual photons. However, given the uncertainties, we cannot rule out a difference up to 15% as is estimated in Ref. [12]. R_γ shows a statistically significant excess of photons above those expected from hadron decays and this excess increases with centrality.

To combine the data sets we apply the corrections calculated from the fast simulation for both the 2007 and 2010 data (after verifying consistency between the corrections calculated for the 2007 data with both the fast Monte Carlo and full GEANT) and average the numerators in Eq. 3 for the 2007 and 2010 data sets. While the correction factor $\langle \varepsilon_\gamma f \rangle$ is different for the two data sets (due to differences in detector dead areas and the different minimum photon energy cuts applied), the systematic uncertainties are the same. Next we determine the direct photon yield from the combined R_γ for each p_T bin:

$$\gamma^{\text{direct}} = (R_\gamma - 1)\gamma^{\text{hadron}}. \quad (4)$$

Here γ^{hadron} is the invariant yield of photons from hadron decays, which we calculate as described above. At this point a systematic uncertainty of 10% on the shape of the input π^0 distribution for the generator needs to be included [26] (this mostly cancels in the denominator of R_γ , but no longer cancels in Eq. 4). The measurement was cross-checked and found consistent with the direct photon spectrum calculated using the fully corrected measured inclusive photon spectrum [26] via the relation $\gamma^{\text{direct}} = (1 - 1/R_\gamma)\gamma^{\text{incl}}$, which has much larger systematic uncertainties because the conversion probability, the e^+e^- pair efficiency and acceptance do not cancel.

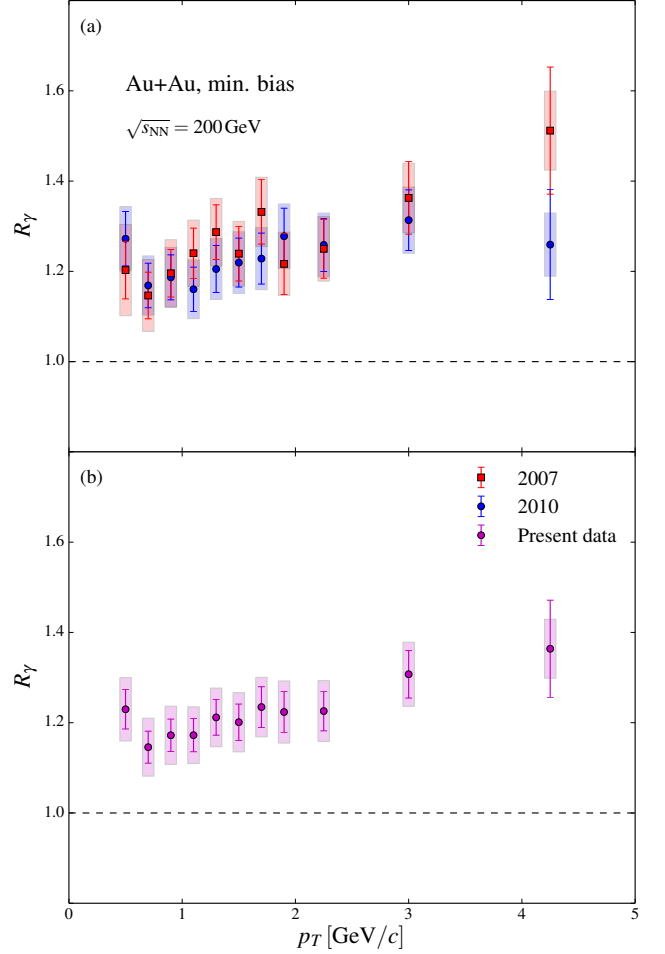


FIG. 4. (a) Ratio R_γ from the 2007 (red open square) and from the 2010 data sets (blue closed circle) in minimum bias Au+Au collisions. Statistical uncertainties are dominated by the π^0 yield extraction. They are plotted as vertical lines. All other systematic uncertainties are added in quadrature and shown as filled boxes. (b) R_γ in the combined 2007+2010 measurement.

The direct photon p_T spectra are shown in Fig. 6 for minimum bias and in Fig. 7 for all centralities. Figure 6 also includes Au+Au data from Ref. [2] and [32]. As a reference, the $p+p$ photon data published by PHENIX, as well as a fit to them, is extrapolated to p_T values below the measured range. The lowest p_T points (open circles) come from a virtual photon measurement [2], while the open squares and open triangles are from the analysis of the 2003 [30] and 2006 $p+p$ data sets [31], respectively. The dashed curve is the joint fit to the $p+p$ data with a functional form $a \left(1 + \frac{p_T^2}{b}\right)^c$. The solid curve is the fit scaled by the corresponding average number of

¹ This shape was used in Ref. [2], including new data in the fit [31] we find parameters $a = (8.3 \pm 7.5) \times 10^{-3}$, $b = 2.26 \pm 0.78$ and

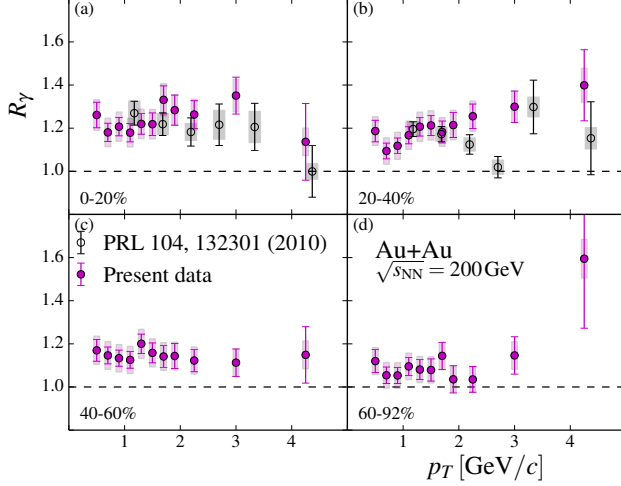


FIG. 5. Ratio R_γ for the combined 2007 and 2010 data sets in centrality bins 0%–20%, 20%–40%, 40%–60% and 60%–92%. Statistical uncertainties plotted as vertical lines are dominated by the π^0 yield extraction. All other systematic uncertainties are added in quadrature and shown as filled boxes. On panels (a) and (b) we also show earlier results from Ref. [2], obtained by extrapolating virtual photons mass to zero.

binary collisions for minimum bias collisions, as calculated from a Glauber Monte Carlo simulation [33]. Below $p_T = 3 \text{ GeV}/c$ an enhancement above the expected prompt production ($p+p$) is observed. The enhancement has a significantly smaller inverse slope than the N_{coll} scaled $p+p$ contribution. Investigating the centrality dependence in more detail (Figure 7) we observe similar behavior. The solid curves are again the $p+p$ fit scaled by the respective number of binary collisions, and they deviate significantly from the measured yields below $3 \text{ GeV}/c$.

TABLE II. The number of nucleon participants N_{part} , number of binary nucleon-nucleon collisions, and constituent-quark participants N_{qp} . Also shown are the values of local inverse slopes in the p_T range 0.6 to $2 \text{ GeV}/c$, cf. Fig. 8.

Centrality	N_{part}	N_{coll}	N_{qp}	$T_{\text{eff}} (\text{MeV}/c)$
0%–20%	279.9 ± 5.7	779.0 ± 75.2	735.2 ± 16.2	$239 \pm 25 \pm 7$
20%–40%	140.4 ± 7.0	296.8 ± 31.1	333.2 ± 12.2	$260 \pm 33 \pm 8$
40%–60%	59.9 ± 5.0	90.6 ± 11.8	126.5 ± 6.8	$225 \pm 28 \pm 6$
60%–92%	17.6 ± 4.2	14.5 ± 4.0	30.2 ± 7.1	$238 \pm 50 \pm 6$

Finally the direct photon contribution from prompt processes (as estimated by the N_{coll} scaled $p+p$ direct photon yield, shown by the curve in Figure 7) is sub-

$c = 3.45 \pm 0.08$. Note that the systematic uncertainties are highly correlated. Also, the lowest actual data point in the fit is at $p_T = 1 \text{ GeV}/c$.

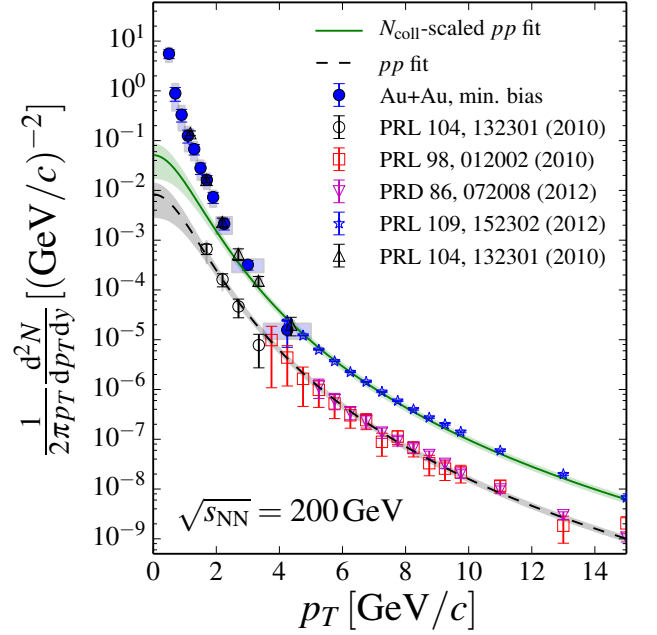


FIG. 6. Direct photon p_T spectra for minimum bias Au+Au from this measurement (solid symbols) and Au+Au and $p+p$ collisions (open symbols). Open circles and triangles: low p_T spectrum obtained with virtual photons in $p+p$ and Au+Au [2]. Open squares and triangles: spectrum with real photons, measured in the EMCAL in $p+p$. Open squares are 2003 data [30], open triangles are 2006 data [31]. Open stars: spectrum with real photons, measured in the EMCAL in Au+Au in 2004 [32]. The dashed line is a fit to the combined set of $p+p$ data, extrapolated below $1 \text{ GeV}/c$, and the solid line the $p+p$ fit scaled with the number of collisions in minimum bias Au+Au. Bands around lines denote 1σ uncertainty intervals in the parametrizations of the $p+p$ data and the uncertainty in N_{coll} , added in quadrature.

tracted to isolate the radiation unique to heavy ion collisions. The results are depicted in Figure 8. While the origin of this additional radiation cannot be directly established (it could be for instance thermal and/or initial state radiation, or the dominant source could even be p_T dependent), it is customary to fit this region with an exponential and characterize the shape with the inverse slope. Accordingly, shown on each panel is a fit to an exponential function in the range $0.6 < p_T < 2 \text{ GeV}/c$. The inverse slopes are approximately $240 \text{ MeV}/c$ independent of centrality, see Table II. In contrast, the yield clearly increases with centrality. We have quantified this by integrating the photon yield above a threshold p_T^{min} , also, we varied the threshold from 0.4 to $1.4 \text{ GeV}/c$ to show that the centrality dependence is not coming from a change of shape at low p_T (see Figure 9).

The yield increases with a power-law function N_{part}^α ; this is illustrated by the linear rise of the yield with N_{part} in the logarithmic representation shown on Figure 9 together with fits to AN_{part}^α . The fit parameters are shown

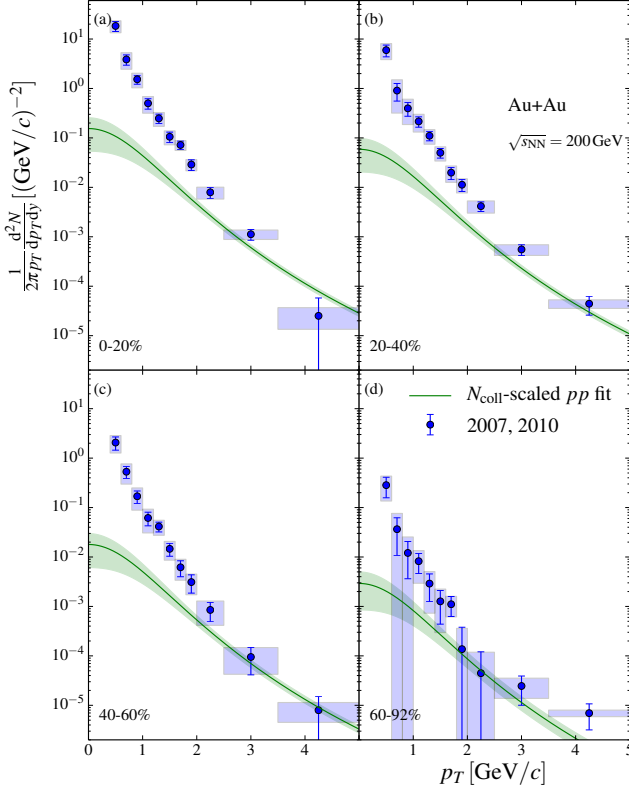


FIG. 7. Direct photon p_T spectra in centrality bins 0%–20%, 20%–40%, 40%–60% and 60%–92%. Widths of filled boxes indicate bin widths in this analysis. The green bands show a N_{coll} -scaled modified power-law fit to the PHENIX $p+p$ data and its extrapolation below 1 GeV/c, cf. Fig. 5. One-sided errors denote 1σ upper limits, other uncertainties are as in Fig. 5.

TABLE III. Fitted parameters from fitting power-law fits $\frac{dN}{dy} = AN_{\text{part}}^\alpha$ for integrated yields with different lower p_T^{ee} limits.

p_T^{min} (GeV/c)	α	A
0.4	$1.47 \pm 0.19 \pm 0.07$	$(2.77 \pm 2.64 \pm 1.41) \times 10^{-3}$
0.6	$1.52 \pm 0.23 \pm 0.15$	$(5.78 \pm 6.64 \pm 5.17) \times 10^{-4}$
0.8	$1.63 \pm 0.22 \pm 0.18$	$(1.68 \pm 1.91 \pm 1.67) \times 10^{-4}$
1.0	$1.45 \pm 0.19 \pm 0.08$	$(1.99 \pm 1.87 \pm 1.28) \times 10^{-4}$
1.2	$1.41 \pm 0.18 \pm 0.08$	$(1.49 \pm 1.37 \pm 0.91) \times 10^{-4}$
1.4	$1.47 \pm 0.20 \pm 0.09$	$(5.00 \pm 5.18 \pm 3.44) \times 10^{-5}$

in Table III. The same power is observed independent of the p_T cutoff, consistent with the spectra having the same shape independent of centrality. A simultaneous fit to the data in Figure 9 results in an average value of $\alpha = 1.48 \pm 0.08(\text{stat}) \pm 0.04(\text{syst})$.

We have also considered the recently suggested scaling with the number of quark participants N_{qp} , which works well for charged particle production [34]. Here N_{qp} is calculated with a Glauber Monte Carlo simulation simi-

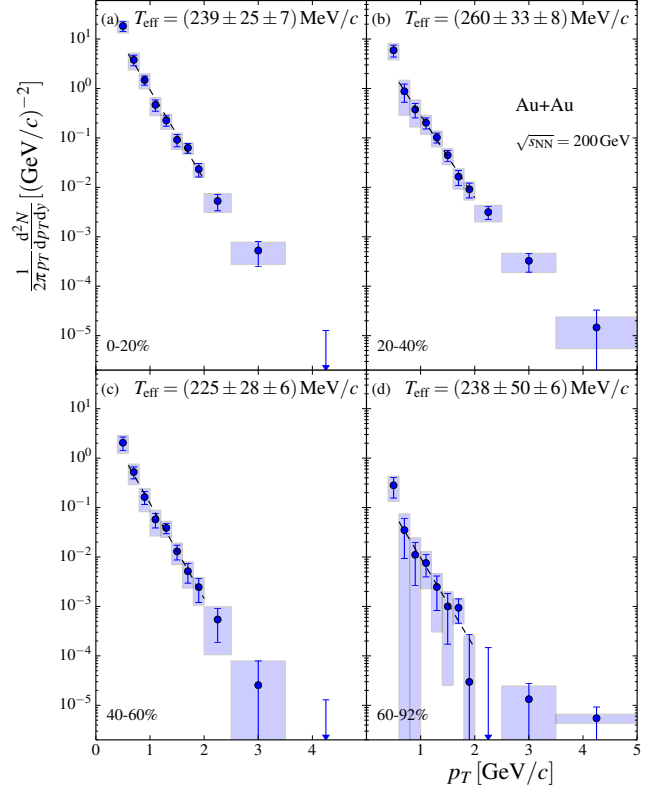


FIG. 8. Direct photon p_T spectra after subtraction of the N_{coll} scaled $p+p$ contribution in centrality bins 0%–20%, 20%–40%, 40%–60% and 60%–92%. Uncertainties are plotted as in Fig. 7. Dashed lines are fits to an exponential function in the range $0.6 \text{ GeV/c} < p_T < 2.0 \text{ GeV/c}$, see Table II for the numerical values.

lar to N_{part} by picking random locations for constituent quarks within the nucleus. While our data is better described by scaling with a power-law in N_{part} , it is also consistent with a power-law function N_{qp}^β , where N_{qp} is the number of quark participants. In this case we find an exponent of $\beta = 1.31 \pm 0.07(\text{stat}) \pm 0.03(\text{syst})$.

In most theoretical models thermal photon emission involves binary collisions of constituents, partons or hadrons, in hot and dense matter. Thus the emission rate from a unit volume should be proportional to the square of the number of constituents, while bulk particle production should scale with the number of constituents [23, 35]. Because particle production is approximately proportional to N_{part} one might expect thermal photon emission to scale as N_{part}^2 times a correction for the increasing reaction volume with centrality. The increasing volume will reduce the centrality dependence, so that one expects $1 < \alpha < 2$ for thermal photon emission.

Recent theoretical studies of the centrality dependence confirm our finding that the yield of thermal photon emission increases approximately with a power law function of N_{part} . In the PHSD transport approach the power α is approximately 1.5 [36], with no evident change in

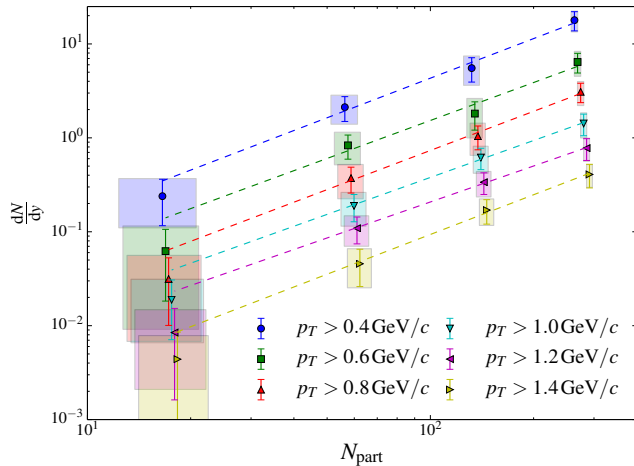


FIG. 9. Integrated thermal photon yields as a function of N_{part} for different lower p_T integration limits. The dashed lines are independent fits to a power-law.

the shape of the spectra with centrality, very similar to our data. A hydrodynamic model [37] shows a power law increase of the yield with a power α in the range from 1.67 to 1.9, increasing monotonically as the lower integration threshold increases from 0.4 to 1.4 GeV/c. Photon production in a glasma phase [22] was predicted to scale with N_{part}^α with $1.47 < \alpha < 2.2$. Other new production mechanisms, proposed to address the large v_2 , have distinctly different centrality dependence. The yield from enhanced thermal photon emission in the strong magnetic field is expected to decrease with centrality, as the strength of the field weakens with decreasing impact parameter [19]. The thermal photon yield should thus increase more slowly than expected from standard processes, but a quantitative estimate is not yet available.

V. SUMMARY AND CONCLUSIONS

We have isolated the low momentum direct photon yield emitted in Au+Au collisions. The shape of the p_T spectra does not depend strongly on centrality, with an average inverse slope of 240 MeV/c in the range from 0.6 to 2 GeV/c. The yield increases with centrality as N_{part}^α

with $\alpha \sim 1.5$. In conclusion, these results will help distinguish between different photon-production mechanisms and will constrain models of the space-time evolution of heavy-ion collisions.

ACKNOWLEDGMENTS

We thank the staff of the Collider-Accelerator and Physics Departments at Brookhaven National Laboratory and the staff of the other PHENIX participating institutions for their vital contributions. We acknowledge support from the Office of Nuclear Physics in the Office of Science of the Department of Energy, the National Science Foundation, Abilene Christian University Research Council, Research Foundation of SUNY, and Dean of the College of Arts and Sciences, Vanderbilt University (U.S.A), Ministry of Education, Culture, Sports, Science, and Technology and the Japan Society for the Promotion of Science (Japan), Conselho Nacional de Desenvolvimento Científico e Tecnológico and Fundação de Amparo à Pesquisa do Estado de São Paulo (Brazil), Natural Science Foundation of China (P. R. China), Croatian Science Foundation and Ministry of Science, Education, and Sports (Croatia), Ministry of Education, Youth and Sports (Czech Republic), Centre National de la Recherche Scientifique, Commissariat à l'Énergie Atomique, and Institut National de Physique Nucléaire et de Physique des Particules (France), Bundesministerium für Bildung und Forschung, Deutscher Akademischer Austausch Dienst, and Alexander von Humboldt Stiftung (Germany), Hungarian National Science Fund, OTKA (Hungary), Department of Atomic Energy and Department of Science and Technology (India), Israel Science Foundation (Israel), National Research Foundation of Korea of the Ministry of Science, ICT, and Future Planning (Korea), Physics Department, Lahore University of Management Sciences (Pakistan), Ministry of Education and Science, Russian Academy of Sciences, Federal Agency of Atomic Energy (Russia), VR and Wallenberg Foundation (Sweden), the U.S. Civilian Research and Development Foundation for the Independent States of the Former Soviet Union, the Hungarian American Enterprise Scholarship Fund, and the US-Israel Binational Science Foundation.

-
- [1] E. V. Shuryak, Phys. Lett. B **78**, 150 (1978).
 - [2] A. Adare *et al.* (PHENIX Collaboration), Phys. Rev. Lett. **104**, 132301 (2010).
 - [3] M. Wilde (for the ALICE Collaboration), Nucl. Phys. A **904-905**, 573c (2013).
 - [4] A. Adare *et al.* (PHENIX Collaboration), Phys. Lett. **109**, 122302 (2012).
 - [5] D. Lohner (ALICE), J. Phys. Conf. Series **446**, 012028 (2013), arXiv:1212.3995 [hep-ex].
 - [6] D. d'Enterria and D. Peressounko, Euro. Phys. J. **46**, 451 (2006).
 - [7] S. Turbide, R. Rapp, and C. Gale, Phys. Rev. C **69**, 014903 (2004).
 - [8] P. Huovinen, P. V. Ruuskanen, and S. S. Räsänen, Phys. Lett. B **535**, 109 (2002).
 - [9] D. K. Srivastava and B. Sinha, Phys. Rev. C **64**, 034902 (2001).
 - [10] J. e. Alam *et al.*, Phys. Rev. C **63**, 021901 (2001).

- [11] F. M. Liu *et al.*, Phys. Rev. C **79**, 014905 (2009).
- [12] K. Dusling and I. Zahed, Phys. Rev. C **82**, 054909 (2010).
- [13] T. Renk, Phys. Rev. C **80**, 014901 (2009).
- [14] H. Holopainen, S. S. Räsänen, and K. J. Eskola, Phys. Rev. C **84**, 064903 (2011).
- [15] A. K. Chaudhuri and B. Sinha, Phys. Rev. C **83**, 034905 (2011).
- [16] H. vanHess, C. Gale, and R. Rapp, Phys. Rev. C **84**, 054906 (2011).
- [17] F. M. Liu, arXiv:1212.6587 (2013).
- [18] K. Kajantie, J. Kapusta, L. McLarren, and A. Mekjian, Phys. Rev. D **34**, 2746 (1986).
- [19] G. Basar, D. E. Kharzeev, and V. Skokov, Phys. Rev. Lett. **109**, 202303 (2012).
- [20] B. Müller, S. Y. Wu, and D. L. Yang, arXiv:1308.6568 (2013).
- [21] V. V. Goloviznin, A. M. Snigirev, and G. M. Zinovjev, (2012), arXiv:1209.2380.
- [22] M. Chiu, T. K. Hemmick, V. Khachatryan, A. Leonidov, and L. McLerran, (2012), arXiv:1202.3679.
- [23] V. Cerny, P. Lichard, and J. Pisut, Z. Phys. C. **31**, 163 (1986).
- [24] K. Adcox *et al.* (PHENIX Collaboration), Nucl. Instrum. Methods **A499**, 469 (2003).
- [25] W. Anderson *et al.* (PHENIX Collaboration), Nucl. Instrum. Methods **A646**, 35 (2011).
- [26] A. Adare *et al.* (PHENIX Collaboration), Phys. Rev. C **81**, 034911 (2010).
- [27] J. Beringer and others (Particle Data Group), Phys. Rev. D **86**, 010001 (2012).
- [28] S. S. Adler *et al.* (PHENIX Collaboration), Phys. Rev. Lett. **96**, 202301 (2006).
- [29] A. Adare *et al.* (PHENIX Collaboration), Phys. Rev. C **87**, 034911 (2013).
- [30] S. S. Adler *et al.* (PHENIX Collaboration), Phys. Rev. Lett. **98**, 012002 (2007).
- [31] A. Adare *et al.* (PHENIX Collaboration), Phys. Rev. D **86**, 072008 (2012).
- [32] S. Afanasiev *et al.* (PHENIX Collaboration), Phys. Rev. Lett. **109**, 152302 (2012).
- [33] M. L. Miller, K. Reygers, S. J. Sanders, and P. Steinberg, Annu. Rev. Nucl. Part. Sci. **57**, 205 (2007).
- [34] A. Adare *et al.* (PHENIX Collaboration), Phys. Rev. C **89**, 044905 (2014).
- [35] D. Teaney and L. Yan, Phys. Rev. C **89**, 014901 (2014).
- [36] O. Linnyk, W. Cassing, and E. Bratkovskaya, Phys. Rev. C **89**, 034908 (2014), arXiv:1311.0279 [nucl-th].
- [37] C. Shen, U. W. Heinz, J.-F. Paquet, and C. Gale, Phys. Rev. C **89**, 044910 (2014), arXiv:1308.2440 [nucl-th].